




Spinning sugars in antigen biosynthesis: characterization of the *Coxiella burnetii* and *Streptomyces griseus* TDP-sugar epimerases

Received for publication, December 19, 2021, and in revised form, April 2, 2022. Published, Papers in Press, April 6, 2022,

<https://doi.org/10.1016/j.jbc.2022.101903>

Alice R. Cross^{1,2}, Sumita Roy^{1,2} , Mirella Vivoli Vega^{1,2}, Martin Rejzek³ , Sergey A. Nepogodiev³ , Matthew Cliff⁴ ,
Debbie Salmon², Michail N. Isupov², Robert A. Field^{3,4}, Joann L. Prior⁵, and
Nicholas J. Harmer^{1,2,*} , on behalf of the GoVV consortium

From the ¹Living Systems Institute, and ²Department of Biosciences, University of Exeter, Exeter, United Kingdom; ³Department of Biological Chemistry, John Innes Centre, Norwich Research Park, Colney Lane, Norwich, United Kingdom; ⁴Manchester Institute of Biotechnology, University of Manchester, Manchester, United Kingdom; ⁵Dstl, Porton Down, Salisbury, Wiltshire, United Kingdom

Edited by Joseph Jez

The sugars streptose and dihydrohydroxystreptose (DHHS) are unique to the bacteria *Streptomyces griseus* and *Coxiella burnetii*, respectively. Streptose forms the central moiety of the antibiotic streptomycin, while DHHS is found in the O-antigen of the zoonotic pathogen *C. burnetii*. Biosynthesis of these sugars has been proposed to follow a similar path to that of TDP-rhamnose, catalyzed by the enzymes RmlA, RmlB, RmlC, and RmlD, but the exact mechanism is unclear. Streptose and DHHS biosynthesis unusually requires a ring contraction step that could be performed by orthologs of RmlC or RmlD. Genome sequencing of *S. griseus* and *C. burnetii* has identified StrM and CBU1838 proteins as RmlC orthologs in these respective species. Here, we demonstrate that both enzymes can perform the RmlC 3",5" double epimerization activity necessary to support TDP-rhamnose biosynthesis *in vivo*. This is consistent with the ring contraction step being performed on a double epimerized substrate. We further demonstrate that proton exchange is faster at the 3"-position than the 5"-position, in contrast to a previously studied ortholog. We additionally solved the crystal structures of CBU1838 and StrM in complex with TDP and show that they form an active site highly similar to those of the previously characterized enzymes RmlC, EvaD, and ChmJ. These results support the hypothesis that streptose and DHHS are biosynthesized using the TDP pathway and that an RmlD paralog most likely performs ring contraction following double epimerization. This work will support the elucidation of the full pathways for biosynthesis of these unique sugars.

The gammaproteobacterium *Coxiella burnetii* evolved recently from tick endosymbionts (1) to become an obligate intracellular pathogen of mammals (2). This bacterium infects a wide range of mammals causing reproductive failures (3, 4). It is a significant economic pathogen of sheep, goats, and cattle

(5), causing spontaneous abortion of pregnancies (6). Humans can be infected by *C. burnetii* either through aerosols or consumption of meat and dairy products (with 1–10 bacteria sufficient to cause disease) (7, 8). *C. burnetii* in unpasteurized ruminant milk poses a particular risk (9–11). Humans generally present with a self-limiting febrile illness (12). A small percentage of cases lead to more serious complications such as miscarriage, hepatitis, or endocarditis (2, 13, 14). *C. burnetii* infection can be effectively treated with doxycycline (2). However, diagnosis is often challenging as *C. burnetii* grows only in highly defined media, requires environment-controlled microaerobic incubators (15), and symptoms of infection are generally nonspecific.

From a "One Health" perspective, a vaccine against *C. burnetii* would be the ideal approach to reduce veterinary and human infection (6). Inactivated whole cell vaccines have proved effective in animals and humans (16, 17). These are not licensed for human use in the USA, EU, or UK as they cause severe reactions in seropositive individuals (18). Current efforts to develop novel vaccines are focused on the development of subunit- (19) or epitope-based vaccines (20, 21). A very strong subunit vaccine candidate is the *C. burnetii* polysaccharide O-antigen. A complete O-antigen is required for immune evasion and efficient infection of mammalian cells (22, 23). Serial passaging of *C. burnetii* selects for mutants that cease producing some or all their O-antigen (24, 25). The most common mutants either lack a polymer of the unusual saccharide virenose ("intermediate") or the entire O-antigen (26) (Fig. 1A). Strains lacking the O-antigen are avirulent in the guinea-pig model of infection (27). The O-antigen is the dominant epitope of WT *C. burnetii* (28), suggesting that any vaccine against *C. burnetii* will require the O-antigen (28). This highlights the importance of a deepened understanding of the biosynthesis of this polysaccharide.

The *C. burnetii* O-antigen characteristically contains two C-3 methylated/hydroxymethylated sugars, virenose and dihydrohydroxystreptose (DHHS; Fig. 1B) (29, 30). Virenose is also found in *Bacillus cereus* and *Streptomyces albaduncus*

* For correspondence: Nicholas J. Harmer, N.J.Harmer@exeter.ac.uk.
Present address for Mirella Vivoli Vega: School of Biochemistry, University of Bristol, Bristol BS8 1TD, U.K.

C. burnetii and S. griseus TDP-sugar epimerases

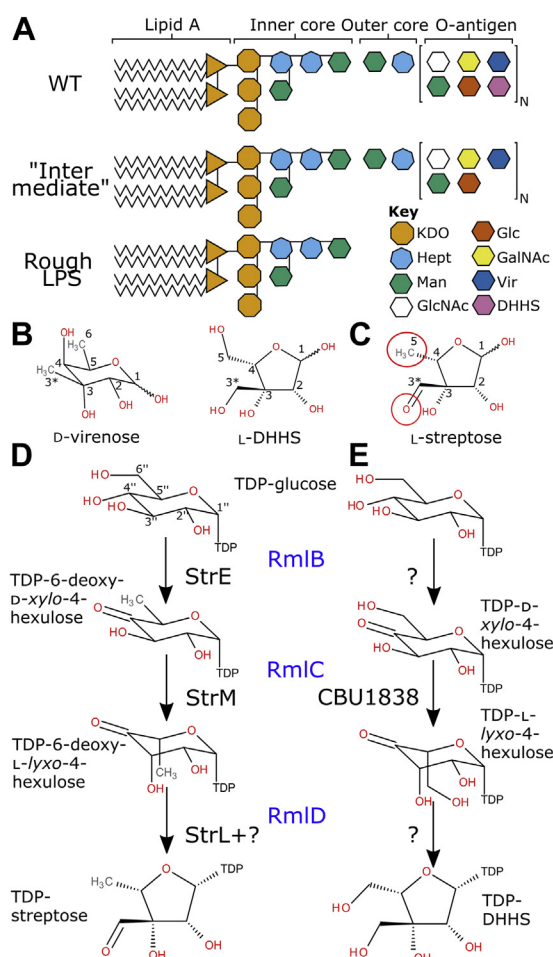


Figure 1. Saccharide structures in *Coxiella burnetii* and related sugars. A, overview of the *C. burnetii* lipopolysaccharide and O-antigen. WT *C. burnetii* makes a smooth LPS with the inner and outer cores and a full O-antigen. Mutants cause either an "intermediate" phenotype without virenose in the O-antigen or a "rough" phenotype lacking the outer core and O-antigen. The linkage of the outer core and O-antigen is not known. Based on (26). B and C, the unusual monosaccharides virenose and dihydrohydroxystreptose (DHHS) from the *C. burnetii* O-antigen (B) and the related sugar streptose (C). The differences between DHHS and streptose are highlighted with red circles. D and E, proposed biosynthetic pathways for TDP-linked streptose (D) and DHHS (E). The equivalent *Escherichia coli* enzymes for each step are shown in blue in between the two panels; proposed enzymes for the *Streptomyces griseus* (34) and *C. burnetii* (this study) pathways, where known, are shown in black. Chemical structures drawn using BIOVIA Draw v16.1. GalNAC, *N*-acetyl-galactosamine; GlcNAC, *N*-acetyl-glucosamine; Glc, glucose; KDO, 2-keto-3-deoxy-*D*-mannoic acid; Man, mannose; Vir, virenose.

(31, 32). Biosynthetic pathways have been proposed in these two organisms, and a similar pathway has been proposed in *C. burnetii* (33). No equivalent pathway has been proposed for DHHS biosynthesis. The most similar known sugar to DHHS is streptose (Fig. 1B), the central saccharide unit of the aminoglycoside antibiotic streptomycin (34), produced by *Streptomyces griseus*. Streptose differs from DHHS in having no hydroxyl at C-6 and being oxidized at the C-3 hydroxymethyl group. Streptose is synthesized from TDP-glucose, in a manner analogous to the biosynthesis of rhamnose (Fig. 1C) (34–37). A reasonable path to DHHS synthesis would involve a C-4 oxidase of TDP-glucose, a 5"-mono or 3",5"-double

epimerase (38), and an enzyme similar to the streptose synthase (37) (Fig. 1, D and E). Although it remains possible that the epimerase might also perform the ring rearrangement, the only precedent for this reaction class was performed by an enzyme from a different structural class (39).

Two regions (*cbu0825* to *cbu0856* and *cbu1831* to *cbu1838*) have been suggested as coding for DHHS synthesizing genes (26). The *cbu1831* to *cbu1838* region contains two genes that show high sequence identity to genes in the rhamnose biosynthesis pathway. CBU1834 has over 60% sequence identity to characterized RmlA orthologs (33) and so is highly likely to be a glucose-1-phosphate thymidyltransferase. TDP-glucose has also been proposed to be a precursor of virenose (33) and so is not necessarily characteristic of DHHS biosynthesis. CBU1838 shows 27 to 53% identity with characterized RmlC orthologs (Table S1). With this sequence identity, this protein is highly likely to be an ortholog of RmlC and act as a TDP-*D*-xylo-4-hexulose 3,5-epimerase. This activity is not required for virenose biosynthesis. As *C. burnetii* does not produce rhamnose, it is unlikely that it would be required for rhamnose biosynthesis. This leaves DHHS biosynthesis as the only reasonable function of CBU1838.

RmlC is part of a family of epimerases that use a deprotonation/reprotonation mechanism (40). RmlC uses a histidine base to deprotonate the substrate and a tyrosine acid to reprotonate from the opposite side of the sugar (41–44). The same residues are likely involved in epimerizing at both 3" and 5" positions: the sugar ring flips between the two reactions to present the second site to be epimerized to the catalytic base and acid (41). These amino acids are highly conserved in the family (Fig. 2). RmlC orthologs have been characterized biochemically and structurally from a range of species (Table 1) (38, 42, 43, 45–49). Paralogs that selectively epimerize at either the 3' or 5' carbon have also been characterized (44, 50, 51). These studies have highlighted likely residues for binding to the TDP carrier (43, 52, 53). For streptose and DHHS biosynthesis, only epimerization at the 5" position is strictly necessary: the C3-C4 bond is broken in the streptose biosynthesis step (35), which will remove the stereocentre at C3. RmlC paralogs for streptose (StrM) and DHHS (CBU1838) biosynthesis have been proposed bioinformatically (33) (e.g., by KEGG (54)); however, such assignments can be inaccurate and so experimental confirmation is desirable (55).

Here, we tested the hypothesis that StrM and CBU1838 are orthologs of RmlC. We expected that they would perform only the epimerization step and not perform the structural rearrangement activity that has yet to be assigned. As both enzymes contain all the catalytic residues proposed for 3",5"-double epimerization, we expected that they might perform both transformations. We demonstrate *in vivo* and *in vitro* that these enzymes are competent to perform the double epimerization. Using NMR, we demonstrate that, surprisingly, proton-deuteron exchange at the 3" position is faster than at the 5" position for both enzymes. The structures of CBU1838 and StrM show that they form an active site highly similar to previously characterized enzymes, in keeping with the biochemical data. These data support a 3",5"-double epimerized substrate for the streptose ring rearrangement.

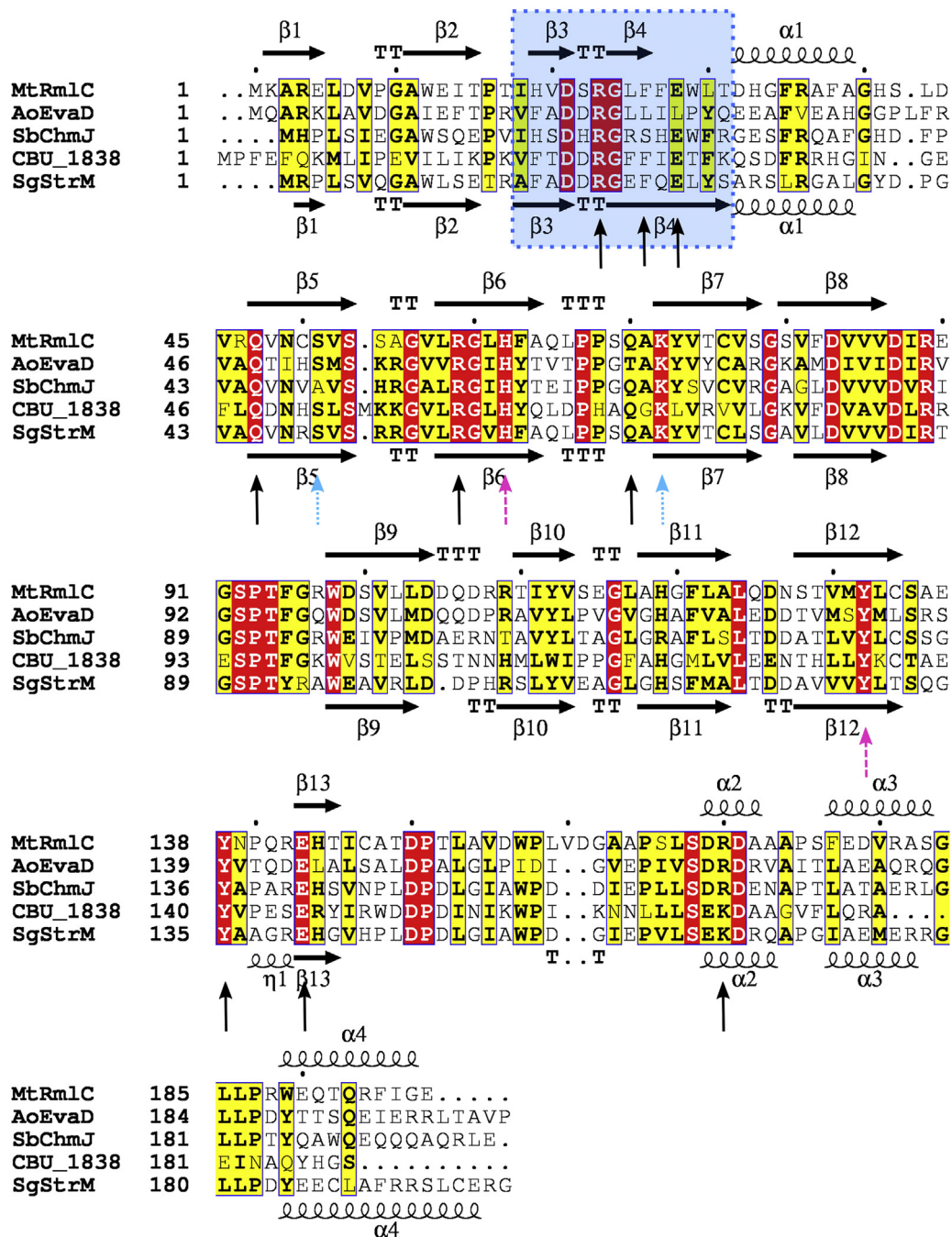


Figure 2. Structural alignment of RmlC paralogs. Alignment generated using Modeller v9.21 (71) from the PDB ID codes 2IXC (41), 1O16 (50) and 4HMZ (44) (*MtRmlC*, *AoEvaD*, and *SbChmJ*, respectively) and the PDB files from *CBU1838* and *SgStrm* solved in this study. Chain A was used in each case. Secondary structure elements for *MtRmlC* and *SgStrm* are noted above and below the sequence alignments, respectively. The strand exchange between chains is highlighted with a blue box. The residues that interact with TDP and citrate and which are likely the catalytic acid and base are indicated with black arrows, sky blue dotted arrows, and pink dashed arrows, respectively. Figure generated using ESPript v3.0222 (72); a red box/white character relates strict identity, a black bold character relates similarity in a group, and filled in yellow characters relates similarity across groups.

Results

CBU1838 complement RmlC in Escherichia coli

We firstly tested whether *CBU1838* can complement the *E. coli* RmlC ortholog RfbC. We cultured WT MG1655 *E. coli* and *rfbC* mutant bacteria, and *rfbC* mutants complemented with *CBU1838*. We extracted soluble small molecules from each culture. WT MG1655 showed negligible levels of TDP-glucose and moderate levels of

TDP-rhamnose. The *rfbC* mutant showed increased TDP-glucose levels and reduced TDP-rhamnose levels (Fig. 3; $p < 0.0001$ and $p < 0.05$ respectively, ANOVA test comparing all tested samples). This is expected for a mutant at this essential step of the pathway. When the *rfbC* mutant was complemented with *CBU1838*, the WT sugar nucleotide levels were restored (Fig. 3). In contrast, complementation with the RmlC paralog *EvaD*, which preferentially epimerizes

C. burnetii and S. griseus TDP-sugar epimerases

Table 1
Summary of existing structures of RmlC paralogs

Reaction	Enzyme activity	EC number	Common name	PDB ID	Species ^a	Ref.
1	TDP-6-deoxy-D-xylo-4-hexulose 3",5"-epimerase	5.1.3.13	RmlC	2IXC/1UPI	Mtu	(41, 46)
				2IXH	Pa	(41)
				1NYW	Ss	(53)
				1EP0	Mth	(45)
				1DZR	Sty	(38)
2	TDP-6-deoxy-D-xylo-4-hexulose 5"-epimerase	N/A	EvaD	3RYK	Ba	(48)
				1O16	Ao	(50)
3	TDP-6-deoxy-D-xylo-4-hexulose 3"-epimerase	5.1.3.27	ChmJ	4HN0	Sb	(44)
				NovW	Sn	(43)
				2COZ	Sn	(43)
4	CDP-6-deoxy-D-xylo-4-hexulose epimerase	N/A	WbcA	5BUV	Ye	(51)
				2PA7	At	(49)
5	TDP-6-deoxy-3,4,keto-hexulose isomerase	5.3.2.4	QdtA	4ZU7	Tt	(47)
				WlaRB	Cj	(47)
				Cj1430	Cj	(42)

Key published structures of proteins with experimentally determined activities.

^a Species abbreviations: Mtu, *Mycobacterium tuberculosis*; Pa, *Pseudomonas aeruginosa*; Ss, *Streptococcus suis*; Mth, *Methanobacterium thermoautotrophicum*; Sty, *Salmonella typhimurium*; Ba, *Bacillus anthracis*; Ao, *Amycolatopsis orientalis*; Sb, *Streptomyces bikiniensis*; Sn, *Streptomyces niveus*; Ye, *Yersinia enterocolitica*; At, *Aneurinibacillus thermoaerophilus*; Tt, *Thermoanaerobacterium thermosaccharolyticum*; Cj, *Campylobacter jejuni*.

the 5" position, was not able to restore WT sugar nucleotide levels. These data gave good confidence that CBU1838 performs both 3" and 5" epimerizations of TDP-6-deoxy-D-xylo-4-hexulose, as expected.

StrM and CBU1838 complement RmlC in vitro

We next tested whether StrM and CBU1838 can perform the function of *E. coli* RmlC in a coupled assay. We used the test enzyme coupled to RmlB and RmlD in a catalytic cascade to convert TDP-glucose to TDP-rhamnose. Both StrM and CBU1838 complemented RmlC in these assays effectively (Fig. 4). Identical concentrations of StrM and RmlC gave a similar effect. A higher concentration of CBU1838 was required to achieve the same effect. This is consistent with the expected function of CBU1838, epimerizing a sugar that retains the 6"-OH group. These data further support the concept that StrM and CBU1838 perform both 3" and 5" epimerizations of TDP-6-deoxy-D-xylo-4-hexulose.

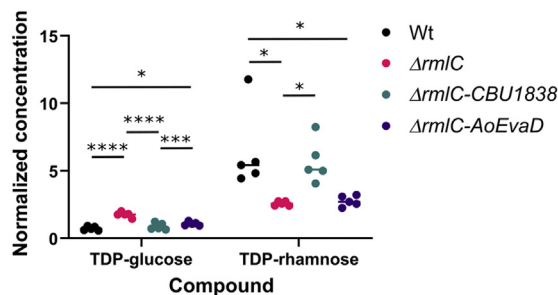


Figure 3. CBU1838 complements *rmlC* in vivo. MG1665 *Escherichia coli*, the Keio collection *rmlC* mutant, and complements of this mutant with CBU1838 and AoEvaD were grown to stationary phase in LB. Cells were harvested and metabolites extracted in 50% (v/v) acetonitrile. Metabolite concentrations were determined by HPLC-MS using a triple-quad instrument. Concentrations were determined by comparison to standards at defined concentrations and normalized to an internal ¹³C-labeled TDP-glucose sample added to all samples. Five experimental replicates were taken for each data point. The bars represent the mean. All points for each compound were compared by ANOVA followed by Tukey's multiple comparison test using Graphpad Prism v.9.2.0. **p* < 0.05; ****p* < 0.0005; *****p* < 0.0001.

CBU1838 shows a reduced rate compared to RmlC and StrM, consistent with its modified substrate

We determined the kinetic constants for StrM and RmlC, in comparison to other characterized enzymes. We used purified TDP-6-deoxy-D-xylo-4-hexulose and coupled the test enzymes to RmlD. Data from StrM, RmlC, CBU1838, and EvaD all fitted very well to the Michaelis–Menten equation, with no evidence of cooperativity (Fig. S1). StrM and RmlC showed a similar *k_{cat}* with StrM having a slightly lower *K_M* (Table 2). CBU1838 showed a lower *k_{cat}* and a clearly higher *K_M* (Table 2). This is consistent with its expected 6"-hydroxy substrate. As expected, the 5"-specific epimerase EvaD showed a substantially lower *k_{cat}*. We did not observe any activity with the 3"-specific epimerase ChmJ (Fig. S2). Previous studies have demonstrated that ChmJ has no 5"-epimerization activity (44), and that the coupling enzyme RmlD only reduces double-epimerized products (56, 57). The kinetic constants provide further evidence that StrM is likely an ortholog of RmlC. CBU1838 can perform this activity, but its likely native substrate is 6"-hydroxylated.

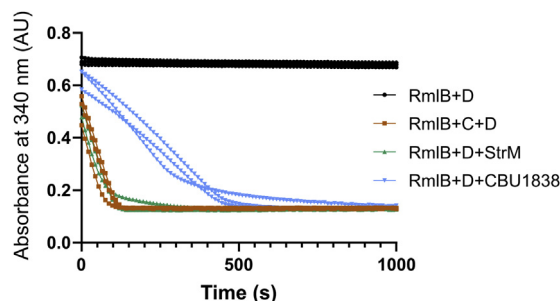


Figure 4. StrM and CBU1838 complement RmlC in vitro. The turnover of TDP-glucose to TDP-rhamnose by RmlB, RmlC, and RmlD was monitored by following the reduction of NADPH at 340 nm. Two hundred micromolar each NADPH and TDP-glucose were incubated with 0.4 μM RmlB and RmlD and as appropriate 0.4 μM RmlC, 0.1 μM StrM, or 1.6 μM CBU1838. StrM and CBU1838 were able to complement RmlC in this assay, albeit at a reduced rate for CBU1838. Three experimental replicates were taken for each condition.

Table 2
Kinetic constants for EcRmlC, SgStrM, CbCBU1838, and AoEvaD

Epimerase	k_{cat} (s^{-1})	K_M (μM)	k_{cat}/K_M ($s^{-1} mM^{-1}$)	R^2
EcRmlC	5.5 ± 0.10	830 ± 40	6.6 ± 0.2	0.996
SgStrM	5.4 ± 0.1	600 ± 40	9.1 ± 0.4	0.988
CBU1838	1.75 ± 0.05	2000 ± 200	0.88 ± 0.04	0.986
AoEvaD	0.39 ± 0.02	632 ± 98	0.63 ± 0.07	0.921

Kinetic data were determined using commercial TDP-6-deoxy-D-xylo-4-hexulose, with the reaction coupled to EcRmlD to allow continuous measurement of the oxidation of NADPH. Data were fitted to the Michaelis–Menten equation using Graphpad v. 8.0 and the fit quality determined from the R^2 value.

RmlC, StrM, and 1838 epimerize at both the 3'' and 5'' positions

To give further confidence in the activity of CBU1838 and StrM, in a novel assay, we monitored their activity directly using NMR and GC-MS without employing a coupling agent. We performed 1H -NMR experiments in deuterated buffer. As RmlC uses a deprotonation-protonation mechanism with different proton acceptors and donors, we expected to observe a loss of signal from protons bound to the 5'' and 3'' carbon atoms. We observed solvent exchange at both positions for RmlC, StrM, CBU1838, and EvaD, with relative rates in the same order as the rates observed in a coupled assay (Figs. 5A and S3). Surprisingly, the rate of exchange at the 3'' position was significantly faster than the rate at the 5'' position for RmlC, StrM, and CBU1838 (Table 3); for EvaD, the rate of exchange at the two positions was similar. When the reaction was permitted to proceed to completion, RmlC, StrM,

and EvaD all showed almost complete exchange at both 3'' and 5'' positions (Fig. 5B). In contrast, the 3'' specific enzyme ChmJ showed almost complete exchange at the 3'' position, with very little exchange observed at the 5'' position. GC-MS analysis of enzyme reactions run to completion confirmed that exchange had occurred at both positions for CBU1838, StrM, and RmlC (Fig. S4). Consistent with the NMR data and previous work (44), ChmJ showed strong exchange at the 3'' position only. These data strongly support a double epimerase activity for both CBU1838 and StrM.

Sugar backbone rearrangement is not observed with either StrM or CBU1838

In neither NMR nor GC-MS data was there any evidence of a rearrangement of the sugar backbone. The proposed biosynthetic pathways of both StrM and CBU1838 require such a rearrangement, catalyzed by either the epimerase or a synthase/reductase for each pathway. Our direct detection of product formation and chemical structure analysis might have allowed us to detect this rearrangement. However, as the five-membered rings are likely to be substantially disfavored at equilibrium, the possibility remains that rearranged structures were present but below the limit of detection.

The structures of StrM and CBU1838 are consistent with their role as double epimerases

We determined the structures of StrM and CBU1838 by X-ray crystallography, in the presence and absence of TDP (Table S2). Both proteins show an overall dimeric architecture consistent with previously solved members of this family (Fig. 6A). Both proteins show a strand exchange in common with orthologs. A phylogenetic tree (Fig. S5) suggests that CBU1838 groups with other 3'',5'' epimerases, while StrM is closer in sequence to the single site epimerases. The sequence identities and structure RMSDs are consistent with this

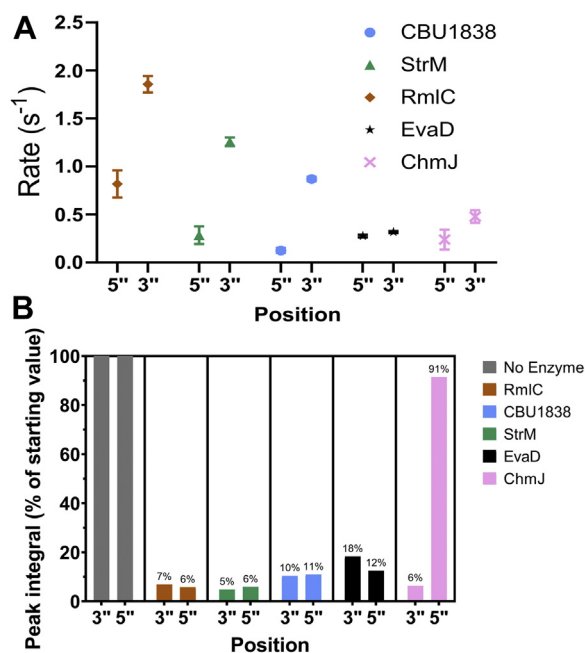


Figure 5. Rate of RmlC paralogs monitored by NMR. RmlC paralogs were incubated with purified TDP-6-deoxy-D-xylo-4-hexulose. A, the loss of proton signal at the 3'' and 5'' positions in the sugar was monitored by NMR. The rate was monitored every 5 to 10 min over 90 min to calculate an initial rate. B, samples were incubated over 18 h to allow the reaction to proceed to completion. RmlC, StrM, and CBU1838 showed almost complete conversion to product in both 3'' and 5'' positions. ChmJ in contrast showed conversion only at the 3'' position. Note that the substrate showed almost no loss of signal over the course of the experiment. Error bars represent the standard error in the mean.

Table 3
Rate of hydrogen-deuterium exchange catalyzed by RmlC paralogs

Epimerase	Rate of H-D exchange (s^{-1})	
	3''	5''
RmlC	1.86 ± 0.08	0.8 ± 0.1
StrM	1.26 ± 0.04	0.28 ± 0.09
CBU1838	0.87 ± 0.02	0.12 ± 0.03
AoEvaD	0.31 ± 0.01	0.28 ± 0.01
ChmJ	0.48 ± 0.07	0.2 ± 0.1

RmlC paralogs were incubated with commercial TDP-6-deoxy-D-xylo-4-hexulose. The loss of proton signal at the 3'' and 5'' positions in the sugar was monitored by NMR. The rate was monitored for up to 90 min to calculate an initial rate.

C. burnetii and S. griseus TDP-sugar epimerases

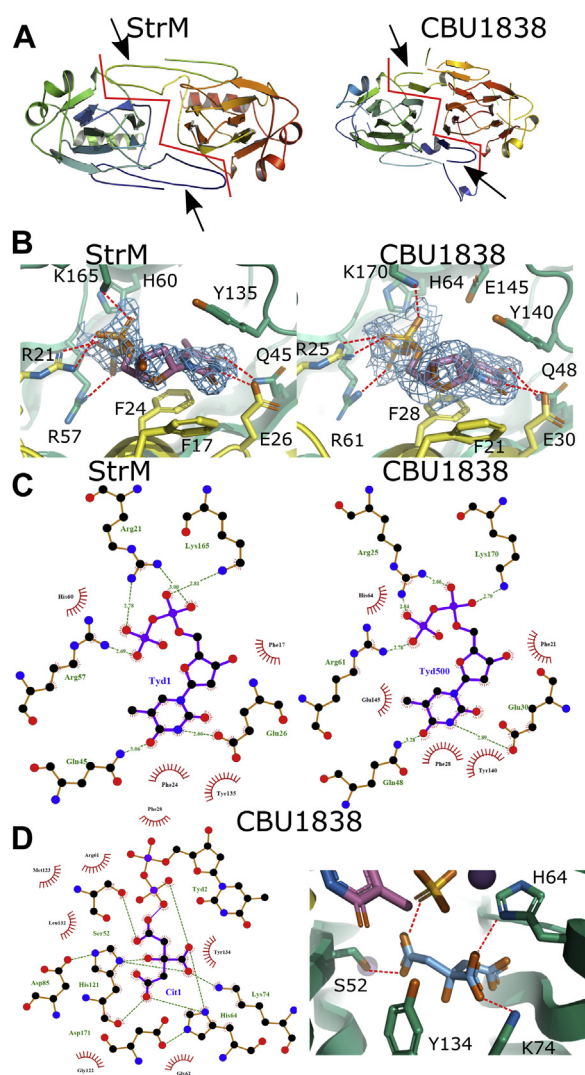


Figure 6. StrM and CBU1838 show expected interactions with ligands. A, ribbon diagram of the structure of StrM (left) and CBU1838 (right). Both proteins form the domain-swapped dimer characteristic of the RmlC proteins. The red lines indicate the dimer interfaces. The domain-swapped strands are indicated by black arrowheads. Proteins are shown in cartoon format, colored blue: protomer 1, N-terminus to red: protomer 2, C-terminus. B and C, structures of both proteins complexed to TDP show a network of interactions conserved with other RmlC enzymes. Interaction maps for TDP with both enzymes were calculated using LigPlus v. 1.4.5 (82). Structures are shown with protein backbone shown as cartoon, with TDP and interacting residues shown as sticks. Colors: nitrogen, blue; oxygen, red; phosphorus, orange; protomer 1 carbon, green; protomer 2 carbon, yellow; TDP carbon, rose. Hydrogen bonds are shown as red dashes. D, a citrate molecule occupies the CBU1838 substrate sugar site and makes interactions with key residues. Left: LigPlus summary of interactions. Right: Structural representation of the citrate. The two conserved catalytic residues H60 and Y130 flank the citrate. Representation as in B, with citrate carbons shown in sky blue. Panels A, B, and D made using PyMOL v. 2.3.4.

(Table S1). TDP binds to both proteins in a similar manner (Fig. 6, B and C). TDP is held in place by a network of amino acid side chains^a (F21*, R25*, F28*, E30*, Q48, R61, H64, Y140, K170) from both protomers (starred residues from the domain swapped strands). Additional interactions are formed through

^a Residue numbers given are for CBU1838. The equivalent residues in StrM are (in order mentioned on this page) F17*, R21*, F24*, E26*, Q45, R57, H60, Y135, and K165; N47, Q68, Y129, and E140; S49 and K70.

bound solvent from N50, Q72, Y134, and E145. These are all strongly conserved across RmlC orthologs (Fig. 2). The CBU1838-TDP structure showed a citrate molecule (carried over from crystallization) bound to the active site. This molecule occupies the same space as the substrate in previously solved structures. The citrate interacts with S52, H64, K74, and Y134 from the protein and TDP (Fig. 6D). These amino acids are well conserved among orthologs, and H64/Y134 are the catalytic base and acid proposed from previous studies (41–44). The conformation of these side chains is very similar to that seen in complexes of other enzymes with substrate analogs (Fig. S6). These structures give further confidence that CBU1838 and StrM are indeed orthologs of RmlC. They have a very similar fold, show clear and specific binding to TDP, and retain the key catalytic residues in the correct orientation.

Discussion

Streptose and DHHS are monosaccharides produced by a single organism each. Both sugars are proposed to be synthesized through modified TDP-rhamnose pathways. *S. griseus* and *C. burnetii* contain putative orthologs of this biosynthetic pathway. Both organisms contain a single TDP-6-deoxy-D-xylo-4-hexulose 3",5"-epimerase ortholog (StrM and CBU1838). We sought to determine whether these enzymes perform both epimerizations and whether either might also perform the sugar ring rearrangement activity. Answering these questions will provide further insight into the biosynthesis of these unusual sugars.

CBU1838 showed robust double epimerase activity both *in vitro* and *in vivo*. CBU1838 complemented an *rfbC* (*rmlC*) mutation, restoring flux through the pathway and consuming cellular TDP-glucose and TDP-6-deoxy-D-xylo-4-hexulose (Fig. 3). CBU1838 and StrM were competent to replace RmlC *in vitro* in a biosynthetic pathway (Fig. 4). It was notable that substantially more CBU1838 was required to restore activity than RmlC or StrM. Similarly, CBU1838 showed a lower k_{cat} and higher K_M than either RmlC or StrM (Table 2). This is consistent with the proposed role of CBU1838, as the DHHS pathway requires a substrate with a 6"-hydroxyl. CBU1838 contains a methionine residue (M123) in place of a phenylalanine conserved among other RmlC orthologs, which would provide space for the hydroxyl. The k_{cat} and K_M values that we obtained for StrM and RmlC are in the same order as those observed for other RmlC paralogs (Table S3). It is notable that our data were collected at 37 °C, while the comparative data were collected at 21 to 25 °C. It is likely that other enzymes would react faster at higher temperatures but might show a higher K_M (58).

Our NMR data show that CBU1838 and StrM have similar activity to *E. coli* RmlC, with CBU1838 again showing a reduced comparative activity. The rate of proton exchange at the 3" position was faster than that at the 5" position for all three enzymes (Fig. 5 and Table 3). The *Mycobacterium tuberculosis* RmlC showed faster epimerization at the 5" position (41). Dong *et al.* suggested that in the likely catalytic conformation, the 5" proton is more acidic than the 3" proton

(41). Our experiments measured the loss of proton signal by NMR, while the previous study measured the product masses by GC-MS. Furthermore, our study used chemically prepared TDP-6-deoxy-D-xylo-4-hexulose, which has only recently become commercially available. This may explain some differences between our study and previous work. We note that as all the reactions involve proton transfers at all steps (40), there may be a strong kinetic isotope effect (59) on either or both epimerizations. As our methods for differentially measuring the two epimerizations rely on deuterium, this confounding effect cannot be excluded.

The structures of CBU1838 and StrM are highly similar to previously solved structures of paralogs from other species. TDP is held in place by residues that are strongly conserved (Figs. 2 and 6) (43, 48, 52). Although we were not able to determine a structure with a TDP-linked sugar, the side chains lining the sugar binding (and catalytic) cavity adopt conformations that are highly similar to those in previous structures (38, 41, 43–45, 48, 50, 51, 53). The proposed catalytic residues, H64 and Y134, occupy a very similar space to the equivalent residues in substrate analog cocrystal structures (41, 53). As their local hydrogen-bonding networks are also conserved, it is likely that they will also be catalytic in these proteins. The presence and conformation of these catalytic residues cannot predict the specificity of the enzymes. While one example of a 5''-specific enzyme showed a mutation that altered the conformation of an important active site side chain (50), 3''-specific epimerases have shown a complete complement of active site residues (44, 51). Our development of a functional assay in *E. coli* allowed us to confirm the activity of StrM and CBU1838 *in vivo* (Fig. 3); although the 5''-specific enzyme EvaD was expressed to the same levels as the active enzymes, it was not competent to complement *rmlC*. However, this assay did not distinguish between StrM (likely a direct RmlC ortholog) and CBU1838 (which is expected to use the 6''-hydroxylated analog).

The evidence presented in this and previous studies strongly suggests that both CBU1838 and StrM act as TDP-4-keto-(6-deoxy)-glucose 3'', 5'' double epimerases. The lower rates observed for CBU1838 are consistent with its natural substrate retaining the 6''-hydroxyl group; an activity to generate this substrate has not yet been identified. This suggests that the streptose and DHHS synthase enzymes (Fig. 1) accept a substrate that is epimerized at both the 3'' and 5'' positions. Although our data suggest that these enzymes cause proton exchange at the 3'' carbon more efficiently than the 5'' carbon, we cannot exclude that the kinetic isotope effect could be confounding. Our results provide powerful evidence that DHHS biosynthesis in *Coxiella* has convergently evolved to use a similar pathway to streptose biosynthesis in *S. griseus*. The key challenge that this presents is to identify the enzymes that provide the two remaining activities to generate DHHS.

Experimental procedures

Gene cloning and synthesis

The gene fragments for *rmlB*, *rmlC*, and *rmlD* were amplified from *E. coli* DH5 α (NEB) genomic DNA (gDNA) by PCR. The *CBU1838* gene fragment was codon-optimized using

IDT's tools and ordered as a gBlock from IDT and amplified by PCR. Primer sequences are provided in Table S4. Gene fragments were cloned into pNIC28-Bsa4 (Addgene #26103, gift of Opher Gileadi, SGC Oxford) using ligation-independent cloning, following published methods (60). Briefly, 16.5 μ g pNIC28-Bsa4 plasmid was digested with 60 U *BsaI* (NEB) in 100 μ l following the manufacturer's protocol and incubated for 2 h at 50 °C. To generate the ligation-independent cloning cohesive ends in both the plasmid and PCR product, a mixture of 1 μ l water, 5 μ l *BsaI*-digested plasmid/PCR-pure DNA, 2 μ l 5X T4 DNA polymerase buffer (Fermentas), 1 μ l 25 mM dGTP (insert) or dCTP (plasmid), 0.5 μ l 100 mM DTT, 0.5 μ l T4 DNA polymerase (Fermentas) was prepared and incubated at 22 °C for 30 min, then 20 min at 75 °C. Two microliters of treated DNA product was added to 1 μ l of treated plasmid. The mixture was incubated at room temperature for 10 min followed by transformation into 5-alpha competent cells (NEB). The *E. coli* DH5 α *rmlD* contains an inactivating point mutation. This was corrected by site-directed mutagenesis using the QuikChange Lightning kit (Agilent), following the manufacturer's instructions.

TDP-sugar epimerase genes for *S. griseus strM*, *Amycolatopsis orientalis evaD*, and *Streptomyces bikiniensis chmJ* were codon optimized using an in-house Python script (<https://github.com/njharmer/CodonOptimise>) and cloned into pET28b with an additional SUMO tag, pET28b, and pET21a respectively by Twist Bioscience. Plasmids were transformed into the expression strain *E. coli* BL21 (DE3) (Novagen) using kanamycin (50 μ g/ml) for selection. For complementation of *E. coli rfbC* mutants, TDP-sugar epimerase genes for *strM*, *evaD*, and *CBU1838* were cloned into the cloning vector pTWIST-A-MC under the control of the lac operon, with a strong ribosome-binding site calculated by the RBS Calculator (De Novo DNA). The Genbank files for all plasmids are available in Supplementary Data.

Preparation of electrocompetent E. coli mutant cell lines and complementation

$\Delta rfbC$ *E. coli* strains (Keio collection; Horizon Discovery #OEC4987-200827372) were grown overnight on LB plates with 50 μ g/ml kanamycin. Colonies were inoculated from LB plates into 10 ml fresh LB broth and incubated overnight at 37 °C with shaking at 225 rpm. One milliliter of overnight culture was inoculated into 100 ml fresh LB medium with kanamycin and incubated at 37 °C with shaking at 225 rpm until A600 was approximately 0.6. Cells were harvested by centrifugation (4200g, 10 min, 4 °C). The cells were resuspended in 40 ml prechilled autoclaved Milli-Q water. Cells were harvested by centrifugation as above and resuspended in 40 ml prechilled autoclaved 10% (v/v) glycerol. A minimum of three 10% glycerol washes were conducted before cells were resuspended in 500 μ l 10% (v/v) glycerol. Complementation plasmids (40 ng) were added to 50 μ l electrocompetent cells, vortexed for 30 s, and incubated on ice for 10 min. The suspension was transferred to a prechilled 0.1 cm electroporation cuvette (Thermo Scientific #5510-11). A single pulse of 1.8 kV was

C. burnetii and S. griseus TDP-sugar epimerases

given by a Gene Pulser Xcell Microbial System (Bio-Rad #1652662). Cells were recovered by adding 1000 μl prewarmed LB medium. The complemented cell suspension was incubated at 37 °C for 1 h shaking at 225 rpm. Transformed cells were grown on LB agar plates supplemented with 100 $\mu\text{g}/\text{ml}$ ampicillin overnight at 37 °C.

Detecting expression of complemented E. coli

Complemented *E. coli* strain colonies were inoculated into 100 ml bottles containing 10 ml LB medium, 100 $\mu\text{g}/\text{ml}$ ampicillin, and incubated overnight at 37 °C with shaking at 225 rpm. One milliliter of each overnight culture was inoculated into individual 500 ml conical flasks containing 100 ml LB medium supplemented with ampicillin and incubated at 37 °C with shaking at 225 rpm. When the A600 reached 0.6, gene expression was induced by adding 200 μM IPTG. Cultures were incubated at 20 °C with shaking at 225 rpm overnight. Fifty milliliter aliquots of overnight cultures were harvested by centrifugation (4500g, 30 min, 4 °C). Cells were lysed using 1 ml BugBuster Master Mix (Millipore #71456-4), following the manufacturer's instructions. The soluble and insoluble fractions were separated by centrifugation at 16,000g for 30 min at 4 °C. Samples were separated on a 4 to 12% ExpressPlus PAGE gel (GenScript #M41212) following the manufacturer's instructions. Samples were transferred to a nitrocellulose membrane (Sartorius Stedim Biotech #11327-41BL) using a Pierce G2 Fast Blotter (Thermo Scientific #15146375) using the preprogrammed protocol. Antibodies were added using an iBind Western device (ThermoFisher #SLF1000), following the manufacturer's recommendations. The primary and secondary antibodies used were anti-penta His (Qiagen #34660) and goat anti-mouse IgG (LiCOR #926-68070) at a dilution of 1:1000. Blots were imaged using an Odyssey Clx imaging system (LiCOR).

Sample preparation for LC-MS QQQ analysis

Complemented *E. coli* strain colonies were inoculated into 100 ml bottles containing 10 ml LB medium, 100 $\mu\text{g}/\text{ml}$ ampicillin for complemented strains, and incubated overnight at 37 °C with shaking at 225 rpm. One milliliter of each overnight culture was inoculated into individual 500 ml conical flasks containing 100 ml LB medium supplemented with kanamycin and ampicillin as necessary and incubated at 37 °C with shaking at 225 rpm until A600 reached 0.6. Expression was induced by adding 200 μM IPTG. Cultures were incubated at 20 °C with shaking at 225 rpm overnight. Fifty milliliter aliquots of overnight cultures were harvested by centrifugation (4500g, 30 min, 4 °C). Cellular contents were extracted into 1 ml 50% (v/v) acetonitrile. Cell suspensions were incubated at 25 °C for 30 min and centrifuged at 20,000g for 30 min at 4 °C. The supernatant was filtered using Millex Non-Sterile Low Protein Binding Hydrophilic LCR (PTFE) Membrane (0.45 μm) filters (Merck #SLLHR04NL) into 1.5 ml MS vials with silicone/PTFE septa and stored at -20 °C for later analysis.

Quantitative LC-MS QQQ analysis:

Quantitative analysis was performed using an Agilent 6420B triple quadrupole (QQQ) mass spectrometer (Agilent Technologies, Palo Alto) coupled to a 1200 series Rapid Resolution HPLC system. Five microliter of sample extract was loaded onto an Agilent Poroshell 120 HILIC-Z, 2.7 μm , 2.1 \times 150 mm analytical column (Agilent Technologies #673775-924). For detection using negative ion mode, mobile phase A comprised 90% (v/v) LC-MS grade acetonitrile with 10 mM ammonium acetate and 5 μM medronic acid, and mobile phase B was 100% water (LC-MS grade) also with 10 mM ammonium acetate and 5 μM medronic acid. The following gradient was used: 0 min – 10% B; 6 min – 35% B; 10 to 13 min – 40% B; 15 min – 10% B; followed by 5 min re-equilibration time at a flow rate of 0.25 ml min⁻¹ with the column held at 25 °C for the duration. The QQQ source conditions for electrospray ionization were as follows: 350 °C gas temperature with a drying gas flow rate of 11 L min⁻¹ and a nebulizer pressure of 35 psig. The capillary voltage was 4 kV.

MS data analysis

Data analysis was undertaken using Agilent MassHunter Quantitative Analysis software (version B.07.01, SP1). Data were normalized to the internal standard, ¹³C TDP-glucose, and the optical density of each culture pre-extraction. TDP-glucose, TDP-rhamnose, GDP-mannose, GDP-fucose, and UDP-glucose concentrations were calculated using standard calibration curves. For the other compounds (where a standard was not available), normalized peak areas were compared.

Expression and purification of TDP-sugar epimerases

RmlB, RmlC, RmlD, StrM, EvaD, and ChmJ were expressed in 500 ml of ZYM-5052 auto-induction media supplemented with 100 $\mu\text{g}/\text{ml}$ kanamycin following the methods of (61). Each flask was inoculated with 10 ml of an overnight culture and grown at 37 °C with agitation at 200 rpm until A600 reached 0.6. Cultures were further incubated at 20 °C for 18 h with agitation. Cells were harvested by centrifugation at 4500g for 30 min at 4 °C. The pellet was resuspended in binding buffer (20 mM Tris-HCl, 500 mM NaCl, 10 mM imidazole, pH 8.0) and lysed by sonication (SONIC Vibra cell VCX130). The sample was clarified by centrifugation (24,000g for 30 min at 4 °C). The soluble fraction was purified using an ÄKTApur chromatography system (Cytiva). The sample was purified using a 1 ml HisTrap crude column (Cytiva). After loading sample, the column was washed with binding buffer, and the protein step eluted into binding buffer supplemented with 250 mM. The eluate was purified over a Superdex 200 pg 16/600 size-exclusion column (Cytiva) and eluted isocratically into 10 mM Hepes, 500 mM NaCl, pH 7.5 (for coupled assays and crystallization) or 10 mM Na_xHPO₄, 500 mM NaCl, pH 7.5 for NMR studies. The eluted protein was concentrated using a Vivaspin centrifugal concentrator (Generon) and stored at -20 °C with 20% (v/v) glycerol for enzymatic assays or stored at -80 °C in small aliquots without any glycerol for crystallization or NMR.

Biochemical assays

The TDP-rhamnose biosynthesis assay coupled the product of RmlC paralogs to RmlD. In brief, reactions were performed in 96-well flat-bottomed plates (Greiner #655001) in a total volume of 200 μ l. For initial studies, reactions consisted of 50 mM Hepes pH 7.5, 20 mM MgCl₂, 350 μ M NADPH, 4 μ M NAD⁺, 0.4 μ M RmlB, 2 μ M RmlC paralog, and 2 μ M RmlD. Reactions were initiated by the addition of 500 μ M TDP-glucose (Carbosynth #MT04383). Reactions were monitored by measurement of the absorbance at 340 nm over 30 min in an Infinite M200 PRO plate reader (Tecan) incubating at 30 °C. For determination of kinetic parameters, RmlB and NAD⁺ were removed and TDP-glucose was replaced with TDP-6-deoxy-D-xylo-4-hexulose (Carbosynth #NT29846) added at a concentration range between 0 to 3 mM (*EcRmlC/SgStrM*) or 0 to 9 mM (CBU1838 or *AoEvaD*). Three experimental replicates were performed for all reactions. Data were fitted to the Michaelis–Menten equation using Graphpad v. 8.1.2.

Deuterium-incorporation analysis by ¹H NMR

Reaction mixtures contained 10 mM MgCl₂, 2.38 mM TDP-6-deoxy-D-xylo-4-hexulose (Carbosynth), and 8 μ M NAD⁺ in a final volume of 250 μ l deuterated 100 mM phosphate buffer pD 7.0. A “zero time” spectrum was recorded without any epimerase. Epimerases (38 nM *EcRmlC*, 46 nM *SgStrM*, 177 nM CBU1838, or 530 nM *AoEvaD*) were added to the above reaction mixture to a final volume of 250 μ l.

All data were collected on a Bruker Neo 600 MHz spectrometer equipped with TCI cryoprobe. Standard Bruker proton experiments were carried out at 298 K (25 °C). Periodic ¹H NMR experiments (64 scans) were carried out in 3 mm NMR tubes. ¹H NMR spectra were recorded every 10 min over a 90 min period, set using the Topspin multi_zgvd command. Later intervals were set manually to record at 2 h, 4 h, 8 h, 18 h, and 24 h, as appropriate. TopSpin 4.0.6 was used for data processing using command ‘efp’ followed by automatic phase correction (‘apk’) and automatic baseline correction (‘abs’). The residual water peak at δ 4.7058 ppm was used as reference for spectra calibration. A set of selected diagnostic signals from no-enzyme control samples was integrated for calibration of the relative abundance of each signal. An integral of H-6 thymidine peak (¹H) was used for peak intensity calibration of the rest of integrals of diagnostic signals, and GraphPad Prism v8.1.2 was used to analyze the data obtained.

Deuterium-incorporation analysis GC-MS

0.5 mg TDP-6-deoxy-D-xylo-4-hexulose (Carbosynth) was incubated in deuterated buffer alone or with the addition of either 1 μ M of *EcRmlB*, *EcRmlC*, *SgStrM*, CBU1838, or *AoEvaD* in 250 μ l final volume. After 18 h, enzymes were inactivated and removed by ethanol precipitation followed by centrifugation at 14,000g for 10 min. Sodium borohydride (~2 mg) was added to each sample for the reduction of keto-moieties followed by incubation at room temperature for 2 h, with shaking at 120 rpm. The reaction was terminated with few drops of glacial acetic acid, followed by 20 μ l 10% (v/v)

acetic acid in methanol. Solvents were evaporated under reduced pressure using GeneVac for 1 h at 35 °C, and 25 μ g myo-inositol was added to the sample as an internal standard. The sugar-nucleotide bond was hydrolyzed by using 250 μ l 2 M TFA followed by incubation at 100 °C for 1.5 h. After cooling the samples, solvents were evaporated again and 100 μ l isopropanol was added before a final evaporation in order to remove the traces of TFA for 1 h.

A second reduction was achieved by addition of 250 μ l 1 M ammonia, containing 10 mg/ml sodium borohydride for 1 h and then 250 μ l acetic acid-methanol (1:9, v/v) was added. The samples were dried under reduced pressure (GeneVac, 1 h at 40 °C) and the addition of acetic acid-methanol followed by drying was repeated once again. This was followed by addition of 250 μ l methanol (without acetic acid) twice with evaporating the solvent off each time (20 min each). The resulting sample was acetylated by incubation at 120 °C for 20 min in a mixture of 100 μ l acetic anhydride and 100 μ l pyridine. After this, approximately 200 μ l toluene was added, and the mixture was concentrated under reduced pressure. The addition of toluene and evaporation was repeated at room temperature.

The alditol acetates were separated by partition between equal volume of methylene chloride and water. After partition, the methylene chloride layer was left to evaporate slowly at room temperature. Finally, samples were dissolved in acetone and analyzed by GC-MS.

Crystallization

Protein concentrations used for crystallization were 5.85 mg/ml (*SgStrM*) and 5.2 mg/ml or 7.8 mg/ml (CBU1838). Crystals were grown using the microbatch method using an Oryx8 crystallization robot (Douglas Instruments). Crystals were grown in hydrophobic plates (Douglas Instruments #VB-Silver-1/1) and covered in a 1:1 mix of paraffin oil and silicone oil (Molecular Dimensions). Crystals were grown either as a 1:1 mixture of protein and mother liquor, or as a 3:2:1 mixture of protein, mother liquor, and seed stocks where seeds had been prepared from previous crystals. The successful cocrystallization conditions, substrates soaking conditions, and cryoprotectants used are detailed in Table S5.

X-ray data collection and structure determination

Data were collected at Diamond Light Source (Didcot) at 100 K using Pilatus 6M-F detectors (Table S2). All data were processed using XDS (62). CBU1838 data were subjected to anisotropic ellipsoidal truncation using the STARANISO server (63). The resolution limit for StrM datasets was set at a point where CC_{1/2} was above 0.3 in the highest resolution shell. CBU1838 data were processed to include regions where the mean I/ σ was systematically above 1.2. Further data processing and structural studies was carried out using the CCP4 program package (64) and the CCP4i2 interface (65). Molecular replacement was used to provide initial phases for datasets using Morda (66) and MolRep (67). The best models for CBU1838 and StrM were 2IXI (41) (54% identity) and 4HMZ (44) (52% identity), respectively. Density fitting was performed

C. burnetii and S. griseus TDP-sugar epimerases

using Coot (68) and refined with REFMAC5 (69). Model validation was carried out with internal modules of CCP4i2 and Coot, employing MolProbity calculations (70).

Data availability

All data underpinning this work are publicly available. Structure coordinates and structure factor files are deposited with the Protein Data Bank (accession numbers: 7PA1, 7P7I, 7P7W, 7P9L, 7P9P, and 7P9Y). Enzymatic and mass spectrometry data are available as Supplementary Files or from Open Research Exeter (doi: <http://doi.org/10.24378/exe.3724>).

Supporting information—This article contains supporting information (38, 41, 43–45, 48, 50, 53, 57, 63, 73–81).

Acknowledgments—The authors thank Simone de Rose (University of Exeter) for assistance with crystallization.

Author contributions—R. A. F., J. L. P., and N. J. H. methodology; A. R. C., S. R., M. V. V., M. R., S. A. N., M. C., and D. S. investigation; A. R. C., S. R., M. V. V., M. R., S. A. N., M. C., D. S., M. N. I., R. A. F., and N. J. H. formal analysis; A. R. C. and N. J. H. writing—original draft; A. R. C., S. R., M. V. V., M. R., S. A. N., M. C., D. S., M. N. I., R. A. F., J. L. P., and N. J. H. writing—review and editing; M. N. I. and N. J. H. data curation; R. A. F., J. L. P., and N. J. H. supervision; R. A. F., J. L. P., and N. J. H. funding acquisition.

Funding and additional information—S. R., M. V. V., R. A. F., and N. J. H. were funded by BBSRC grant BB/N001591/1. A. R. C. and N. J. H. were funded by BBSRC grant BB/M016404/1 and by Dstl grant DSTLX-1000098217. Work at the John Innes Centre (M. R., S. A. N., R. A. F.) was supported by the UK BBSRC Institute Strategic Program on Molecules from Nature—Products and Pathways [BBS/E/J/000PR9790] and the John Innes Foundation, and the InnovateUK: IBCatalyst (Grant BB/M02903411).

Conflict of interest—The authors declare that they have no conflicts of interest with the contents of this article.

Abbreviations—The abbreviations used are: DHHS, dihydrohydroxystreptose.

References

1. Duron, O., Noel, V., McCoy, K. D., Bonazzi, M., Sidi-Boumedine, K., Morel, O., Vavre, F., Zenner, L., Jourdain, E., Durand, P., Arnathau, C., Renaud, F., Trape, J. F., Biguezoton, A. S., Cremaschi, J., et al. (2015) The recent evolution of a maternally-inherited endosymbiont of ticks led to the emergence of the Q fever pathogen, *Coxiella burnetii*. *PLoS Pathog.* **11**, 101511
2. Eldin, C., Melenotte, C., Mediannikov, O., Ghigo, E., Million, M., Edouard, S., Mege, J. L., Maurin, M., and Raoult, D. (2017) From Q fever to *Coxiella burnetii* infection: A paradigm change. *Clin. Microbiol. Rev.* **30**, 115–190
3. Duncan, C., Kersh, G. J., Spraker, T., Patyk, K. A., Fitzpatrick, K. A., Massung, R. F., and Gelatt, T. (2012) *Coxiella burnetii* in northern Fur seal (*Callorhinus ursinus*) Placentas from St. Paul island, Alaska. *Vector-Borne Zoonot.* **12**, 192–195
4. Gonzalez-Barrío, D., and Ruiz-Fons, F. (2019) *Coxiella burnetii* in wild mammals: A systematic review. *Transbound. Emerg. Dis.* **66**, 662–671
5. Mori, M., and Roest, H. J. (2018) Farming, Q fever and public health: Agricultural practices and beyond. *Arch. Public Health* **76**, 2
6. Cross, A. R., Baldwin, V. M., Roy, S., Essex-Lopresti, A. E., Prior, J. L., and Harmer, N. J. (2019) Zoonoses under our noses. *Microbes Infect.* **21**, 10–19
7. Clark, N. J., and Magalhaes, R. J. S. (2018) Airborne geographical dispersal of Q fever from livestock holdings to human communities: A systematic review and critical appraisal of evidence. *BMC Infect. Dis.* **18**, 218
8. Tigertt, W. D., Benenson, A. S., and Gochenour, W. S. (1961) Airborne Q fever. *Bacteriol. Rev.* **25**, 285–293
9. Anastacio, S., Carolino, N., Sidi-Boumedine, K., and da Silva, G. J. (2016) Q fever dairy herd status determination based on serological and molecular analysis of bulk tank milk. *Transbound. Emerg. Dis.* **63**, e293–e300
10. Muskens, J., van Engelen, E., van Maanen, C., Bartels, C., and Lam, T. J. (2011) Prevalence of *Coxiella burnetii* infection in Dutch dairy herds based on testing bulk tank milk and individual samples by PCR and ELISA. *Vet. Rec.* **168**, 79
11. Ryan, E. D., Wrigley, K., Hallinan, A., McGrath, G., and Clegg, T. A. (2018) Antibodies to *Coxiella burnetii* in Irish bulk tank milk samples. *Vet. Rec.* **182**, 550
12. Raoult, D., Marrie, T. J., and Mege, J. L. (2005) Natural history and pathophysiology of Q fever. *Lancet Infect. Dis.* **5**, 219–226
13. Million, M., and Raoult, D. (2017) No such thing as chronic Q fever. *Emerg. Infect. Dis.* **23**, 856–857
14. Seddon, O., Ashrafi, R., Duggan, J., Rees, R., Tan, C., Williams, J., Carson, G., and Healy, B. (2016) Seroprevalence of Q fever in patients undergoing heart valve replacement surgery. *J. Heart Valve Dis.* **25**, 375–379
15. Boden, K., Wolf, K., Hermann, B., and Frangoulidis, D. (2015) First isolation of *Coxiella burnetii* from clinical material by cell-free medium (ACCM2). *Eur. J. Clin. Microbiol.* **34**, 1017–1022
16. Taurel, A. F., Guatteo, R., Joly, A., and Beaudou, F. (2012) Effectiveness of vaccination and antibiotics to control *Coxiella burnetii* shedding around calving in dairy cows. *Vet. Microbiol.* **159**, 432–437
17. Zuckerman, J. N., Van Damme, P., Van Herck, K., and Loscher, T. (2003) Vaccination options for last-minute travellers in need of travel-related prophylaxis against hepatitis A and B and typhoid fever: A practical guide. *Trav. Med Infect Dis.* **1**, 219–226
18. Kazar, J., Brezina, R., Palanova, A., Tvrdá, B., and Schramek, S. (1982) Immunogenicity and reactogenicity of a Q fever chemovaccine in persons professionally exposed to Q fever in Czechoslovakia. *Bull. World Health Organ.* **60**, 389–394
19. J.E. Samuel, E.J. Van Schaik and A.E. Gregory, U.P. Office. Vaccine for immunization against Q-fever. US patent application US10967055B2. 2019.
20. Reeves, P. M., Paul, S. R., Sluder, A. E., Brauns, T. A., and Poznansky, M. C. (2017) Q-Vaxcelerate: A distributed development approach for a new *Coxiella burnetii* vaccine. *Hum. Vacc. Immunother.* **13**, 2977–2981
21. Scholzen, A., Richard, G., Moise, L., Baeten, L. A., Reeves, P. M., Martin, W. D., Brauns, T. A., Boyle, C. M., Raju Paul, S., Bucala, R., Bowen, R. A., Garritsen, A., De Groot, A. S., Sluder, A. E., and Poznansky, M. C. (2019) Promiscuous coxiella burnetii CD4 epitope clusters associated with human recall responses are candidates for a novel T-cell targeted multi-epitope Q fever vaccine. *Front. Immunol.* **10**, 207
22. Downs, C. M. (1968) Phagocytosis of *Coxiella burnetii*, phase I and phase II by peritoneal monocytes from normal and immune Guinea pigs and mice. *Zentralbl. Bakteriol. Orig.* **206**, 329–343
23. van Schaik, E. J., Chen, C., Mertens, K., Weber, M. M., and Samuel, J. E. (2013) Molecular pathogenesis of the obligate intracellular bacterium *Coxiella burnetii*. *Nat. Rev. Microbiol.* **11**, 561–573
24. Hackstadt, T. (1986) Antigenic variation in the phase I lipopolysaccharide of *Coxiella burnetii* isolates. *Infect. Immun.* **52**, 337–340
25. Kersh, G. J., Oliver, L. D., Self, J. S., Fitzpatrick, K. A., and Massung, R. F. (2011) Virulence of pathogenic *Coxiella burnetii* strains after growth in the absence of host cells. *Vector Borne Zoonotic Dis.* **11**, 1433–1438
26. Beare, P. A., Jeffrey, B. M., Long, C. M., Martens, C. M., and Heinzen, R. A. (2018) Genetic mechanisms of *Coxiella burnetii* lipopolysaccharide phase variation. *PLoS Pathog.* **14**, e1006922
27. Moos, A., and Hackstadt, T. (1987) Comparative virulence of intra- and interstrain lipopolysaccharide variants of *Coxiella burnetii* in the Guinea pig model. *Infect. Immun.* **55**, 1144–1150

28. Beare, P. A., Unsworth, N., Andoh, M., Voth, D. E., Omsland, A., Gilk, S. D., Williams, K. P., Sobral, B. W., Kupko, J. J., Porcella, S. F., Samuel, J. E., and Heinzen, R. A. (2009) Comparative genomics reveal extensive transposon-mediated genomic plasticity and diversity among potential effector proteins within the genus *Coxiella*. *Infect. Immun.* **77**, 642–656
29. Amano, K., Williams, J. C., Missler, S. R., and Reinhold, V. N. (1987) Structure and biological relationships of *Coxiella burnetii* lipopolysaccharides. *J. Biol. Chem.* **262**, 4740–4747
30. Schramek, S., Radziejewskalebrecht, J., and Mayer, H. (1985) 3-C-Branched aldoses in lipopolysaccharide of phase-I *Coxiella-burnetii* and their role as immunodominant factors. *Eur. J. Biochem.* **148**, 455–461
31. Kharel, M. K., Nybo, S. E., Shepherd, M. D., and Rohr, J. (2010) Cloning and characterization of the ravidomycin and chrysomycin biosynthetic gene clusters. *Chembiochem* **11**, 523–532
32. Li, Z., Mukherjee, T., Bowler, K., Namdari, S., Snow, Z., Prestridge, S., Carlton, A., and Bar-Peled, M. (2017) A four-gene operon in *Bacillus cereus* produces two rare spore-decorating sugars. *J. Biol. Chem.* **292**, 7636–7650
33. Flores-Ramirez, G., Janecek, S., Miernyk, J. A., and Skultety, L. (2012) In silico biosynthesis of virenose, a methylated deoxy-sugar unique to *Coxiella burnetii* lipopolysaccharide. *Proteome Sci.* **10**, 67
34. Flatt, P. M., and Mahmud, T. (2007) Biosynthesis of aminocyclitol-aminoglycoside antibiotics and related compounds. *Nat. Prod. Rep.* **24**, 358–392
35. Bruton, J., and Horner, W. H. (1966) Biosynthesis of streptomycin. 3. Origin of the carbon atoms of streptose. *J. Biol. Chem.* **241**, 3142–3146
36. Giraud, M. F., and Naismith, J. H. (2000) The rhamnose pathway. *Curr. Opin. Struct. Biol.* **10**, 687–696
37. Wahl, H. P., and Grisebach, H. (1979) Biosynthesis of streptomycin. dTDP-dihydrostreptose synthase from *Streptomyces griseus* and dTDP-4-keto-L-rhamnose 3,5-epimerase from *S. griseus* and *Escherichia coli* Y10. *Biochim. Biophys. Acta* **568**, 243–252
38. Giraud, M. F., Leonard, G. A., Field, R. A., Berling, C., and Naismith, J. H. (2000) RmlC, the third enzyme of dTDP-L-rhamnose pathway, is a new class of epimerase. *Nat. Struct. Biol.* **7**, 398–402
39. Savino, S., Borg, A. J. E., Dennig, A., Pfeiffer, M., de Giorgi, F., Weber, H., Dubey, K. D., Rovira, C., Mattevi, A., and Nidetzky, B. (2019) Deciphering the enzymatic mechanism of sugar ring contraction in UDP-apiose biosynthesis. *Nat. Catal.* **2**, 1115–1123
40. Van Overtveldt, S., Verhaeghe, T., Joosten, H. J., van den Bergh, T., Beereus, K., and Desmet, T. (2015) A structural classification of carbohydrate epimerases: From mechanistic insights to practical applications. *Biotechnol. Adv.* **33**, 1814–1828
41. Dong, C., Major, L. L., Srikannathasan, V., Errey, J. C., Giraud, M. F., Lam, J. S., Graninger, M., Messner, P., McNeil, M. R., Field, R. A., Whitfield, C., and Naismith, J. H. (2007) RmlC, a C3' and C5' carbohydrate epimerase, appears to operate via an intermediate with an unusual twist boat conformation. *J. Mol. Biol.* **365**, 146–159
42. Huddleston, J. P., Anderson, T. K., Girardi, N. M., Thoden, J. B., Taylor, Z., Holden, H. M., and Raushel, F. M. (2021) Biosynthesis of d-glycero-l-gluco-Heptose in the capsular polysaccharides of *Campylobacter jejuni*. *Biochemistry* **60**, 1552–1563
43. Jakimowicz, P., Tello, M., Meyers, C. L., Walsh, C. T., Buttner, M. J., Field, R. A., and Lawson, D. M. (2006) The 1.6-Å resolution crystal structure of NovW: A 4-keto-6-deoxy sugar epimerase from the novobiocin biosynthetic gene cluster of *Streptomyces spheroides*. *Proteins* **63**, 261–265
44. Kubiak, R. L., Phillips, R. K., Zmudka, M. W., Ahn, M. R., Maka, E. M., Pyeatt, G. L., Roggensack, S. J., and Holden, H. M. (2012) Structural and functional studies on a 3'-epimerase involved in the biosynthesis of dTDP-6-deoxy-D-allose. *Biochemistry* **51**, 9375–9383
45. Christendat, D., Saridakis, V., Dharamsi, A., Bochkarev, A., Pai, E. F., Arrowsmith, C. H., and Edwards, A. M. (2000) Crystal structure of dTDP-4-keto-6-deoxy-D-hexulose 3,5-epimerase from *Methanobacterium thermoautotrophicum* complexed with dTDP. *J. Biol. Chem.* **275**, 24608–24612
46. Kantardjiev, K. A., Kim, C. Y., Naranjo, C., Waldo, G. S., Lekin, T., Segelke, B. W., Zemla, A., Park, M. S., Terwilliger, T. C., and Rupp, B. (2004) *Mycobacterium tuberculosis* RmlC epimerase (Rv3465): A promising drug-target structure in the rhamnose pathway. *Acta Crystallogr. D Biol. Crystallogr.* **60**, 895–902
47. Li, Z. Z., Riegert, A. S., Goneau, M. F., Cunningham, A. M., Vinogradov, E., Li, J., Schoenhofen, I. C., Thoden, J. B., Holden, H. M., and Gilbert, M. (2017) Characterization of the dTDP-Fuc3N and dTDP-Qui3N biosynthetic pathways in *Campylobacter jejuni* 81116. *Glycobiology* **27**, 358–369
48. Shornikov, A., Tran, H., Macias, J., Halavaty, A. S., Minasov, G., Anderson, W. F., and Kuhn, M. L. (2017) Structure of the *Bacillus anthracis* dTDP-L-rhamnose-biosynthetic enzyme dTDP-4-dehydro-rhamnose 3,5-epimerase (RfbC). *Acta Crystallogr. F Struct. Biol. Commun.* **73**, 664–671
49. Thoden, J. B., Vinogradov, E., Gilbert, M., Salinger, A. J., and Holden, H. M. (2015) Bacterial sugar 3,4-Ketoisomerases: Structural insight into product stereochemistry. *Biochemistry* **54**, 4495–4506
50. Merkel, A. B., Major, L. L., Errey, J. C., Burkart, M. D., Field, R. A., Walsh, C. T., and Naismith, J. H. (2004) The position of a key tyrosine in dTDP-4-Keto-6-deoxy-D-glucose-5-epimerase (EvaD) alters the substrate profile for this RmlC-like enzyme. *J. Biol. Chem.* **279**, 32684–32691
51. Salinger, A. J., Brown, H. A., Thoden, J. B., and Holden, H. M. (2015) Biochemical studies on WbcA, a sugar epimerase from *Yersinia enterocolitica*. *Protein Sci.* **24**, 1633–1639
52. Dhaked, D. K., Bala Divya, M., and Guruprasad, L. (2019) A structural and functional perspective on the enzymes of *Mycobacterium tuberculosis* involved in the L-rhamnose biosynthesis pathway. *Prog. Biophys. Mol. Biol.* **145**, 52–64
53. Dong, C., Major, L. L., Allen, A., Blankenfeldt, W., Maskell, D., and Naismith, J. H. (2003) High-resolution structures of RmlC from *Streptococcus suis* in complex with substrate analogs locate the active site of this class of enzyme. *Structure* **11**, 715–723
54. Kanehisa, M., Sato, Y., Kawashima, M., Furumichi, M., and Tanabe, M. (2016) KEGG as a reference resource for gene and protein annotation. *Nucleic Acids Res.* **44**, D457–D462
55. Koller, F., and Lassak, J. (2021) Two RmlC homologs catalyze dTDP-4-keto-6-deoxy-D-glucose epimerization in *Pseudomonas putida* KT2440. *Sci. Rep.* **11**, 11991
56. Blankenfeldt, W., Kerr, I. D., Giraud, M. F., McMiken, H. J., Leonard, G., Whitfield, C., Messner, P., Graninger, M., and Naismith, J. H. (2002) Variation on a theme of SDR. dTDP-6-deoxy-L-lyxo-4-hexulose reductase (RmlD) shows a new Mg²⁺-dependent dimerization mode. *Structure* **10**, 773–786
57. Graninger, M., Nidetzky, B., Heinrichs, D. E., Whitfield, C., and Messner, P. (1999) Characterization of dTDP-4-dehydro-rhamnose 3,5-epimerase and dTDP-4-dehydro-rhamnose reductase, required for dTDP-L-rhamnose biosynthesis in *Salmonella enterica* serovar Typhimurium LT2. *J. Biol. Chem.* **274**, 25069–25077
58. Arcus, V. L., Prentice, E. J., Hobbs, J. K., Mulholland, A. J., Van der Kamp, M. W., Pudney, C. R., Parker, E. J., and Schipper, L. A. (2016) On the temperature dependence of enzyme-catalyzed rates. *Biochemistry* **55**, 1681–1688
59. Anderson, V. E. (1992) Isotope effects on enzyme-catalyzed reactions. *Curr. Opin. Struct. Biol.* **2**, 757–764
60. Savitsky, P., Bray, J., Cooper, C. D., Marsden, B. D., Mahajan, P., Burgess-Brown, N. A., and Gileadi, O. (2010) High-throughput production of human proteins for crystallization: The SGC experience. *J. Struct. Biol.* **172**, 3–13
61. Studier, F. W. (2005) Protein production by auto-induction in high density shaking cultures. *Protein Expr. Purif.* **41**, 207–234
62. Kabsch, W. (2010) Xds. *Acta Crystallogr. D Biol. Crystallogr.* **66**, 125–132
63. Tickle, I. J., Flensburg, C., Keller, P., Paciorek, W., Sharff, A., Vornrhein, C., and Bricogne, G. (2018) *Staranis*, Global Phasing Ltd, Cambridge
64. Winn, M. D., Ballard, C. C., Cowtan, K. D., Dodson, E. J., Emsley, P., Evans, P. R., Keegan, R. M., Krissinel, E. B., Leslie, A. G., McCoy, A., McNicholas, S. J., Murshudov, G. N., Pannu, N. S., Potterton, E. A., Powell, H. R., et al. (2011) Overview of the CCP4 suite and current developments. *Acta Crystallogr. D Biol. Crystallogr.* **67**, 235–242

C. burnetii and S. griseus TDP-sugar epimerases

65. Potterton, L., Agirre, J., Ballard, C., Cowtan, K., Dodson, E., Evans, P. R., Jenkins, H. T., Keegan, R., Krissinel, E., Stevenson, K., Lebedev, A., McNicholas, S. J., Nicholls, R. A., Noble, M., Pannu, N. S., *et al.* (2018) CCP4i2: The new graphical user interface to the CCP4 program suite. *Acta Crystallogr. D Struct. Biol.* **74**, 68–84
66. Vagin, A., and Lebedev, A. (2015) MolPro, an automatic molecular replacement pipeline. *Acta Crystallogr. A* **71**, S19
67. Vagin, A., and Teplyakov, A. (2010) Molecular replacement with MOLREP. *Acta Crystallogr. D Biol. Crystallogr.* **66**, 22–25
68. Emsley, P., Lohkamp, B., Scott, W. G., and Cowtan, K. (2010) Features and development of Coot. *Acta Crystallogr. D Biol. Crystallogr.* **66**, 486–501
69. Murshudov, G. N., Skubak, P., Lebedev, A. A., Pannu, N. S., Steiner, R. A., Nicholls, R. A., Winn, M. D., Long, F., and Vagin, A. A. (2011) REFMAC5 for the refinement of macromolecular crystal structures. *Acta Crystallogr. D Biol. Crystallogr.* **67**, 355–367
70. Chen, V. B., Arendall, W. B., 3rd, Headd, J. J., Keedy, D. A., Immormino, R. M., Kapral, G. J., Murray, L. W., Richardson, J. S., and Richardson, D. C. (2010) MolProbity: All-atom structure validation for macromolecular crystallography. *Acta Crystallogr. D Biol. Crystallogr.* **66**, 12–21
71. Webb, B., and Sali, A. (2016) Comparative protein structure modeling using MODELLER. *Curr. Protoc. Protein Sci.* <https://doi.org/10.1002/cpps.20>
72. Gouet, P., Robert, X., and Courcelle, E. (2003) ESPript/ENDscript: Extracting and rendering sequence and 3D information from atomic structures of proteins. *Nucleic Acids Res.* **31**, 3320–3323
73. Karplus, P. A., and Diederichs, K. (2012) Linking crystallographic model and data quality. *Science* **336**, 1030–1033
74. Vaguine, A. A., Richelle, J., and Wodak, S. J. (1999) SFCHECK: A unified set of procedures for evaluating the quality of macromolecular structure-factor data and their agreement with the atomic model. *Acta Crystallogr. D Biol. Crystallogr.* **55**, 191–205
75. Williams, C. J., Headd, J. J., Moriarty, N. W., Prisant, M. G., Videau, L. L., Deis, L. N., Verma, V., Keedy, D. A., Hintze, B. J., Chen, V. B., Jain, S., Lewis, S. M., Arendall, W. B., 3rd, Snoeyink, J., Adams, P. D., *et al.* (2018) MolProbity: More and better reference data for improved all-atom structure validation. *Protein Sci.* **27**, 293–315
76. Sivendran, S., Jones, V., Sun, D., Wang, Y., Grzegorzewicz, A. E., Scherman, M. S., Napper, A. D., McCammon, J. A., Lee, R. E., Diamond, S. L., and McNeil, M. (2010) Identification of triazinoindol-benzimidazolones as nanomolar inhibitors of the Mycobacterium tuberculosis enzyme TDP-6-deoxy-d-xylo-4-hexopyranosid-4-ulose 3,5-epimerase (RmlC). *Bioorg. Med. Chem.* **18**, 896–908
77. Edgar, R. C. (2021) MUSCLE v5 enables improved estimates of phylogenetic tree confidence by ensemble bootstrapping. *bioRxiv*, 2021.2006.2020.44916911.
78. Goddard, T. D., Huang, C. C., Meng, E. C., Pettersen, E. F., Couch, G. S., Morris, J. H., and Ferrin, T. E. (2018) UCSF ChimeraX: Meeting modern challenges in visualization and analysis. *Protein Sci.* **27**, 14–25
79. Kirkpatrick, P. N., Scaife, W., Hallis, T. M., Liu, H.-W., Spencer, J. B., and Williams, D. H. (2000) Characterisation of a sugar epimerase enzyme involved in the biosynthesis of a vancomycin-group antibiotic. *Chem. Comm.*, 1565–1566
80. Stern, R. J., Lee, T. Y., Lee, T. J., Yan, W., Scherman, M. S., Vissa, V. D., Kim, S. K., Wanner, B. L., and McNeil, M. R. (1999) Conversion of dTDP-4-keto-6-deoxyglucose to free dTDP-4-keto-rhamnose by the rmlC gene products of Escherichia coli and Mycobacterium tuberculosis. *Microbiology (Reading)* **145**, 663–671
81. York, W. S., Davill, A. G., McNeil, M., Stevenson, T. T., and Albersheim, P. (1986) Isolation and characterization of plant cell walls and cell wall components. *Methods Enzymol.* **118**, 3–40
82. Laskowski, R. A., and Swindells, M. B. (2011) LigPlot+: Multiple ligand-protein interaction diagrams for drug discovery. *J. Chem. Inf. Model.* **51**, 2778–2786